Polymer 49 (2008) 2728–2737

Contents lists available at ScienceDirect

Polymer

journal homepage: www.elsevier.com/locate/polymer

Experimental characterisation and constitutive modelling of RTM-6 resin under impact loading

Robert Gerlach*, Clive R. Siviour, Nik Petrinic, Jens Wiegand

University of Oxford, Department of Engineering Science, Parks Road, Oxford OX1 3PJ, United Kingdom

ARTICLE INFO

Article history:
Received 12 February 2008
Received in revised form 9 April 2008
Accepted 10 April 2008
Available online 13 April 2008

Keywords:
RTM-6 Resin
Hopkinson bar pulse shaping
Constitutive Modelling

ABSTRACT

The response to mechanical loading of the thermosetting resin system RTM-6 has been investigated experimentally as a function of strain rate and a constitutive model has been applied to describe the observed and quantified material behaviour. In order to determine strain rate effects and to draw conclusions about the hydrostatic stress dependency of the material, specimens were tested in compression and tension at strain rates from 10^{-3} to 10^{4} s^{-1}. A Standard screw-driven tensile machine was used for quasi-static testing, with an 'in house' hydraulic rig and Hopkinson bars for medium and high strain rates, respectively. At all rates appropriate photography and optical metrology have been used for direct strain measurement, observation of failure and validation of experimental procedures. In order to enable the experimental characterisation of this brittle material at very high rates in tension, a novel pulse shaping technique has been applied. With the help of this device, strain rates of up to 3800 s^{-1} have been achieved while maintaining homogeneous deformation state until specimen fracture in the gauge section of the tensile specimens. The yield stress and initial modulus increased with increasing strain rate for both compression and tension, while the strain to failure decreased with strain rate in tension. An existing constitutive model, the Goldberg model has been extended in order to take into account the nonlinear strain rate dependence of the elastic modulus. The model has been validated against 3-point impact bending tests of prismatic RTM-6 beams.

1. Introduction

Thermosetting polymers, such as HEXCEL RTM-6, are networked polymers in which chain motion is restricted by a high degree of cross-linking, and are generally much stronger and more temperature resistant than thermoplastic materials. One of the major applications of thermosetting polymers is their use as a matrix material for a wide variety of modern fibre reinforced polymers (FRPs) in the aerospace, automotive, marine, oil and gas industries [1–3]. RTM-6 is a one component system especially developed for the aerospace industry and is widely used as a matrix in composite materials. In particular, the system is designed for the resin transfer moulding (RTM) production processes.

The importance of characterising and modelling the response of this matrix to loading at different strain rates has become apparent due to the development of 3D fibre reinforced composite materials, in which the usual 'in-plane' fibres are augmented by some form of reinforcement in the 'out of plane' direction. In these composites, the matrix volume content can reach up to 50%, and large matrix pockets can be formed at meso-scale (tow level, Fig. 1). The influence of these pockets on the strain rate dependency, the deformation of fibre tows or damage behaviour of the 3-D composite has only received limited attention [4]. Furthermore, the variety of different matrix systems available for 3-D composites creates the opportunity to investigate the optimal choice: to find the most desirable combination of matrix properties and select a resin system that best matches this combination for particular applications. One approach to investigate this issue is by means of virtual testing at meso-scale using a finite element model of the constituents (tows and matrix). It is therefore necessary to understand the behaviour of the matrix material in detail and to apply an appropriate constitutive model capturing important characteristics of the matrix that contribute to the global response of the final composite material.

This approach is currently restricted, as the dynamic response of thermosets is not yet fully understood. No data for RTM-6 have been published for high rates of strain in either compression or tension; data on other resin materials are also limited and generally restricted to compressive behaviour only. It is therefore important to provide the growing research community focusing on virtual models at meso-scale level with accurate experimental data on the most common matrix systems, especially since the question as to what extent dynamic compressive behaviour could be used as a reference for derivation of tensile properties still needs to be answered.

* Corresponding author. Tel.: +44 1865 283475; fax: +44 1865 273906.
E-mail address: robert.gerlach@eng.ox.ac.uk (R. Gerlach).

0032-3861/$ – see front matter © 2008 Elsevier Ltd. All rights reserved.
doi:10.1016/j.polymer.2008.04.018

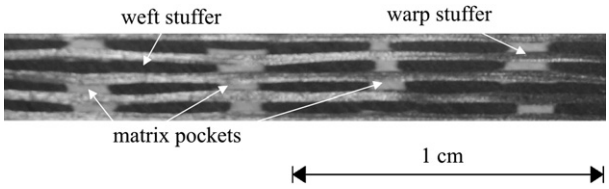

Fig. 1. Cross section of a 3D woven composite showing distribution of matrix pockets.

A constitutive model suitable for virtual tests must capture the nonlinear, strain rate dependent and hydrostatic stress dependent material behaviour of the polymer. Furthermore, it should be possible to account for the different failure behaviours in compression and tension. An additional criterion is ease of calibration and numerical efficiency, especially as virtual modelling tackles increasingly complex problems.

The present study therefore includes a comprehensive experimental characterisation of the strain rate dependent and hydrostatic stress dependent material response of RTM-6. Special focus was given to the brittle behaviour of the resin at high rates in tension. With the help of a novel pulse shaping technique, strain rates not yet reported could be achieved while maintaining valid testing conditions (failure in the gauge section and homogeneous strain field). An existing constitutive model, the Goldberg model [5], has been applied and extended to take into account the nonlinear strain rate dependency of the elastic modulus. This model has been calibrated against the characterisation experiments and validated against 3-point impact bending tests of RTM-6 beams.

1.1. Measurement of the constitutive response of brittle materials with a low sound speed at high rates of strain

Compared to metals, only very limited data are available for strain rate sensitivity of polymers in general and resins in particular [5–9]. Furthermore, most of the published data on resins deal with compression only. Generally, these tests show an increase in modulus and failure stress with increasing strain rate. The small data set for tension can be explained by the various difficulties in performing high strain rate characterisation experiments on resins with pronounced hydrostatic stress effects and comparably brittle response in tension, as well as a low sound speed (<2000 m/s). Reported results indicate that the brittle behaviour in tension is much more pronounced than in compression [5,7,8], but high rates of strain (above 500 s^{-1}) have rarely been achieved and no data could be found for strain rates in excess of 1500 s^{-1}. Additionally, most of the published high strain rate data in tension are of questionable benefit since tensile specimens tend to fail outside the gauge section and the data produced have unacceptably large scatter.

This paper therefore describes novel experimental techniques that have been developed to increase the understanding of the tensile behaviour of resins at high rates of strain. Characterisation experiments were performed successfully using a tensile Hopkinson bar modified with a pulse shaper. Brazilian tests were also considered, but found to be unsuitable for this material. Nevertheless, these tests are briefly described. The data from these experiments, as well as traditional compressive experiments at different rates of strain, were used to calibrate the Goldberg model. In order to validate a constitutive polymer model, additional experiments at a larger scale are often used in order to exercise the model with a variety of stress states and failure modes. Components [10], disc impact [11] and three point bending tests on notched beams [12] have been reported. For this study, an unnotched 3-point impact bending test [13] was used, and results comparing experimental data to model predictions are presented in this paper.

1.2. Constitutive modelling of thermosetting resins

The traditional approach to modelling polymers usually adopts viscoelastic models such as the Maxwell model and the Kelvin/Voigt model to describe the time dependent behaviour while modified von Mises or Tresca yield criteria capture the pressure sensitivity [14,15]. Recently, more advanced models that are able to predict nonlinear behaviour of polymers have been developed for both small and large strain formulations (see Refs. [7,16,17] for more detailed information). In particular, the large strain formulation Buckley model [7,18] has been successfully extended to represent strain rate dependency in resins and is able to accurately predict strain softening in compression. However, the expected material behaviour of 3-D composites suggests that the focus of a polymer model for an application in virtual testing of FRPs should be on strain rate dependency in general and hydrostatic pressure sensitivity in particular. A small-strain formulation with a less complex material model and a sound failure criterion may be sufficient.

The basis of this study has been the recently developed Goldberg model which describes the nonlinear response of polymers by relying on the theory which describes viscous flow in liquids. This model has been successfully applied to several glassy polymers [5,19–22]. A distinct advantage of this model compared to many existing models using complex large strain formulations is its accuracy in the small-strain regime and the manageable number of material constants needed to be determined experimentally (only 6 compared to up to 16 constants for other polymer models). It is, furthermore, comparably straightforward to implement into explicit FE codes such as LS-DYNA. The main disadvantage of this small-strain formulation compared to a large strain formulation such as the Buckley model lies in the inability to capture strain softening in compression. The effect of this shortcoming on modelling the global behaviour of a FRP is assumed to be negligible, however, since shear failure in the yarns will most likely occur well before large compression strains are achieved in the matrix pockets. For these reasons, the Goldberg model has been chosen as a basis for this research.

2. Experiments

2.1. Material and specimen design

The thermoset tested in this programme, Hexcel RTM-6, is optimised for RTM-processing (air-tight conditions under pressure), but can be used in open moulds as well. The raw sample material consisted of 10 mm thick plates produced under RTM conditions and 9 mm diameter rods produced by moulding. The cure cycle used was 2 °C/min heating to 130 °C, 1 h dwell at 130 °C, 1 °C/min heating to 180 °C and finally 2 h cure at 180 °C. Final properties are independent of heating rate and dwell temperature, provided that the final cure of 2 h at 180 °C is used, resulting in identical mechanical properties for both sources of material.

The material was characterised under three loading configurations: quasi-uniaxial compression, uniaxial tension and 3-point bending. The specimens for compression tests were right cylinders designed such that the effect of inertia on the measured stresses during high strain rate compression is minimised. Following the Gorham formulation [23], the applied ratio of radius r to height h of the manufactured cylinders is

$$h = \left(\frac{\sqrt{3}}{2}\right) r. \tag{1}$$

The tensile specimens were dog-bone shaped, produced by adhesively bonding a polymer cylinder into a hollow M12 threaded steel rod and subsequent grinding of the gauge section. The final geometry was found after a number of iterations explained below.

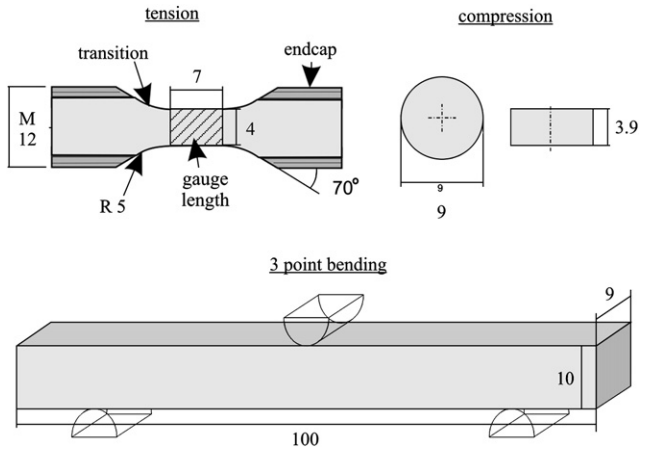

Fig. 2. Specimen dimensions for compression, tension and 3-point bending; all dimensions are in millimetres. For compression experiments above 4000 s^{-1} specimens of 6 mm diameter and 2.6 mm length were used.

The 3-point bend specimens are simple beams cut out of the resin plate. All specimen dimensions can be found in Fig. 2.

2.2. Loading and data acquisition devices

Experiments were performed in three strain rate regimes: quasi-static ($\dot{\varepsilon} \approx 3\text{–}6 \times 10^{-4}\ s^{-1}$); medium ($\dot{\varepsilon} \approx 10\text{–}100\ s^{-1}$); and high ($\dot{\varepsilon} \approx 1000\text{–}6000\ s^{-1}$).

For quasi-static testing, a commercial screw-driven Hounsfield tensile testing machine was used. All experiments were performed with a cross-head velocity of up to 2×10^{-5} m/s in tension or compression as required. A high precision laser extensometer (FIEDLER Optoelektronik, model P-50, resolution 0.1 μm) was used for displacement measurement. These data were then used to calculate the strain and strain rate in the gauge section as functions of time for each individual experiment. Force measurements were made using a calibrated load cell. A high-resolution camera capable of taking one picture every 4 s was used to examine crack propagation patterns and to correlate failure phenomena with the corresponding points on the stress–strain curves. Illumination for the cameras was provided by LED lights with appropriate filters to prevent interference between the cameras and the laser extensometer. It should be noted that in the compression experiments the displacement measurement points were on the loading anvils, as close as possible to the specimen. In tensile experiments measurements were performed on the specimen surface. The effect of this is that there is a tendency to under predict the specimen modulus in compression tests, whilst the modulus in tension is accurate. Because the focus of this study was on high strain rate and post-yield behaviour, short specimens were used to (a) prevent buckling and (b) enable stress equilibrium at high strain rates.

For medium strain rates an in house hydraulic system was used. A strain gauge based load cell is used to measure the force supported by the specimen during loading, and two methods were employed for displacement measurements. The first was an LVDT system measuring the relative movement of the endcaps (tension) or loading anvils (compression), the second was a high speed camera used to monitor the gauge length displacement by tracking two white stripes attached to the specimen (tension) or anvils (compression).

The high-rate experiments were performed using the split Hopkinson compression bar (SHPB) and tension bar (SHTB) discussed in Ref. [7], see Fig. 3. In these systems a compressive or tensile stress wave is produced, using a gas gun driven striker, and travels down the input bar to the specimen. At the interfaces between the

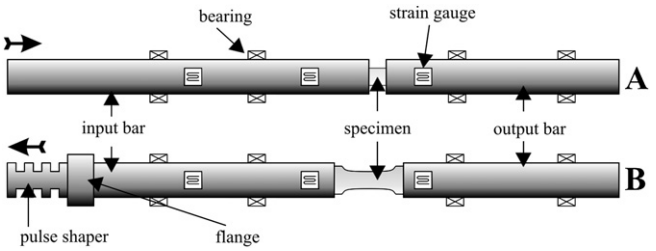

Fig. 3. Split Hopkinson pressure bar (A) and split Hopkinson tensile bar (B). Arrows represent loading provided by a gas gun driven striker, directly in compression, or via a loading bar in tension.

loading bars and the specimen, the stress wave separates into reflected and transmitted components at the input and output ends, respectively. The strains in the bars as functions of time are recorded using two strain gauge stations on the input bar and one on the output bar. The stresses and velocities at the interfaces between the input and output bars and the specimen are calculated using a standard analysis outlined in Ref. [24]. These values are used to obtain the forces and displacements on the specimen's ends. The average specimen strain, as a function of time, is calculated from these displacements; the specimen stress is calculated by further time shifting the forces to the middle of the specimen gauge length taking into account the travel time between the end of the input bar and the beginning of the output bar. A further displacement measurement was performed using high speed photography. In compression, stripes were painted on the ends of the bars, and, as expected, the displacement of these confirmed the results of the standard analysis. In the tensile experiments, speckles were painted onto the specimen surface, enabling displacement to be calculated as a function of position (on the specimen) and time using image correlation [25,26], see Fig. 10. Again, this direct measurement means that specimen strains are more accurately calculated in the tensile experiments than in the compressive.

Three point bend experiments were performed using the Hounsfield machine for quasi-static loading and an impact bending system, based on *the Hopkinson* bar technique, for high-rate loading [13,27]. In this device, an instrumented titanium rod (the impactor) with a wedge-shaped tip is propelled into the centre of a beam shaped specimen, which is supported rigidly at its two ends. The impactor is held in low friction bearings and is initially at rest. A gas gun is used to propel a striker into the impactor; the striker and impactor are of the same material and dimensions, so this theoretically causes the impactor to travel unstressed into the specimen. During the experiment the axial strains within the impactor bar are recorded by means of 4 strain gauges arranged in a single strain gauge station halfway down the bar, and converted into a voltage using an uncompensated Wheatstone bridge. The same methodology as described by Ref. [24] is applied and the force, velocity and thus displacement at the tip of the impactor are obtained as functions of time. Knowing the displacement of the impactor, and assuming a rigid support, the deflection of the specimen is given. Furthermore, an energy balance can be drawn and the amount of energy dissipated due to inelastic deformation and fracture can be estimated. The results of these experiments were quantitatively compared to those from LS-DYNA simulations, thus validating the constitutive model.

The techniques so-far described are quite typical for low, medium and high strain rate material characterisation. However, in order to fully characterise the resin material, further techniques were developed as described below.

2.2.1. Challenges for uniaxial tensile testing of epoxy resins

The difficulty in testing resins in tension arises from several characteristics of these materials. Firstly, they are brittle, resulting

in a very high sensitivity to surface irregularities and bending [7]. A crack that will be suppressed from growing further in compression will result in abrupt failure in tension, and a comparably large scatter in supported stress is inevitable. Furthermore, dog-bone tensile specimens tend to break at random places outside the gauge section [7] or immediately after the transition from the loading bar to the specimen [22], resulting in an invalid test. Results with two cracks along the gauge section have been achieved for strain rates up to 680 s^{-1} [8], where the existence of two cracks has been argued to be an indicator for mechanical equilibrium.

An alternative possibility for measurement of tensile strength of brittle materials over a range of strain rates is the Brazilian test [28,29]. It is often used for concrete and short fibre or particle reinforced polymers. However, tests performed in this study showed that although brittle in tensile tests, the RTM-6 resin does not form tensile cracks at all in Brazilian tests performed using anvils with 11 mm radius, and only does so using flat anvils after a large portion of the specimen has undergone considerable plastic deformation (Fig. 4). Apart from the fact that the resin exhibits some plastic deformation in tension, the hydrostatic stress sensitivity results in increased failure strength during the Brazilian test, and it was concluded that this technique is therefore not applicable to RTM-6.

An improvement on the tensile Hopkinson bar apparatus and the specimen design therefore needs to be undertaken in order to generate high strain rate tensile data. Four factors were identified that contribute to the invalidity of tensile tests performed so far: stress concentrations in the specimens, too long a gauge length, a very short rise time of the input stress wave and a considerable initial peak on this wave. Initially, specimen design was investigated (see Fig. 2). Preliminary specimens were produced with a large radius of curvature, 20 mm, in the transition region between the endcaps and the specimen gauge length; the gauge length was 9 mm. These specimens showed a tendency to fail at the transition between the endcap and the resin rod even at the slowest possible strain rates on the split Hopkinson tensile bar, forming a cavity within the endcap (Fig. 5A); this occurred despite a 70° angle machined in the endcap. A shortened gauge section (of 7 mm) along with a reduced radius of curvature of 5 mm was therefore adopted, and the strain rate at which this cavity occurred increased to 600 s^{-1}, with occasional failure closer towards the gauge section (Fig. 5B). A further increase of strain rate was achieved by adopting pulse shaping techniques. The aim of these techniques is to increase the rise time of the input wave, and they are often applied to split Hopkinson compression bars; for example, by using dummy specimens [30] or pre-loading bars [31]. A recent study on Epon 828/T-403 epoxy made use of a split Hopkinson tensile bar pulse shaping technique, utilising modified striker and incident bars, and strain rates of 1200 s^{-1} were achieved [8]. For the current study, a form of pre-loading bar has been developed which sits at the end of the input bar (see Figs. 3 and 6).

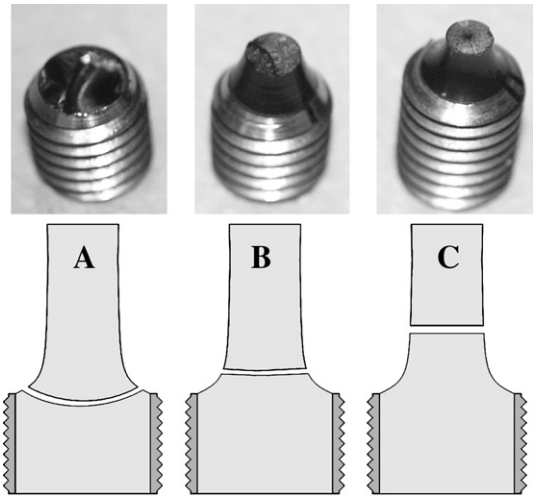

Fig. 5. Failure modes of RTM-6 tensile specimens: (A) failure in endcap; (B) failure in transition region; (C) failure in gauge section.

The pre-loading bar is a flanged rod in which several modest impedance jumps result in parts of the input wave being reflected, leading to an increased rise time of the stress pulse. There is a further impedance jump due to the flange connecting the pulse shaper and the input bar. The effect of the pulse shaper is to increase the rise time of the input signal, and therefore also smooth the stress peak, caused by Pochhammer–Chree oscillations of the input signal. The chosen geometry of the rod is shown in Fig. 6 and the effect of this device can be seen in Fig. 7. Using this device, it was possible to increase the achievable strain rates to 3800 s^{-1}, whilst reliably failing the specimen in the gauge section (Fig. 5C).

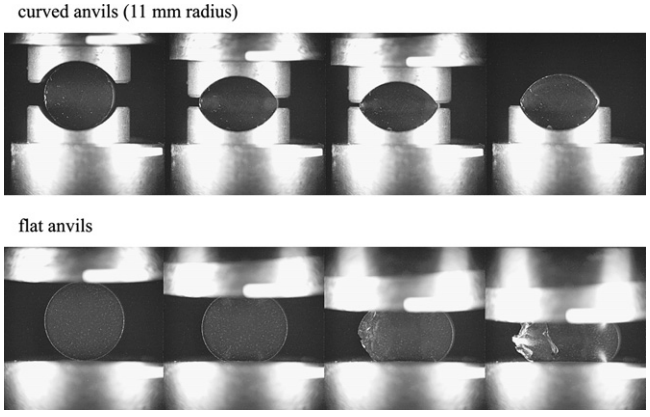

Fig. 4. Plastic deformation of RTM-6 under Brazilian test conditions with curved and flat anvils.

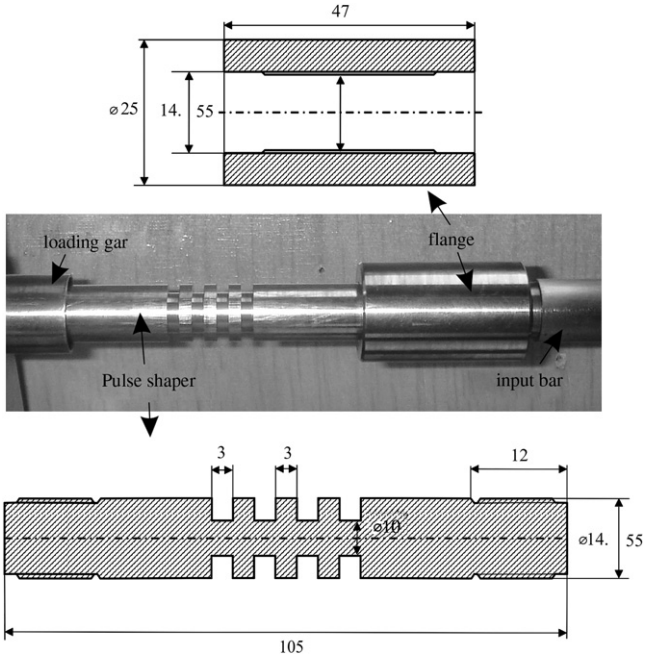

Fig. 6. Pulse shaper geometry, for overview of the connection to the split Hopkinson tensile bar see Fig. 3.

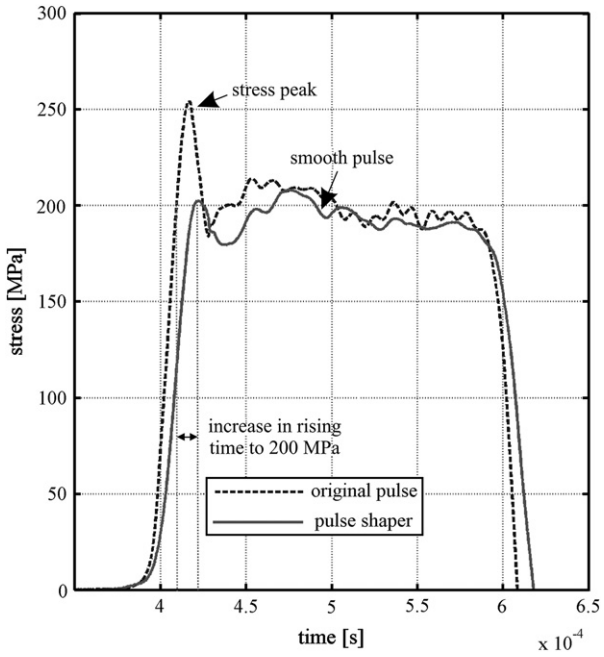

Fig. 7. Influence of the pulse shaper on the input stress wave.

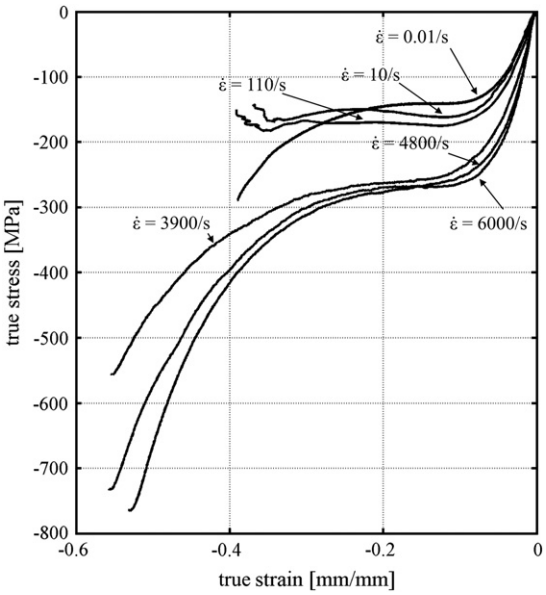

Fig. 9. Representative stress–strain curves at 6 selected strain rates in compression.

2.3. Results in compression and tension

In order to ensure that friction between the anvils and the specimen is minimised, the anvils were carefully polished and the lubricant "Castrol LMX Grease" was used for all compression experiments. Fig. 10 shows a photographic record of the deformation at two strain rates, where no significant barrelling occurred up to the point of failure. For all high-rate tests stress equilibrium was confirmed by comparing the stress at the end of the input bar with that at the end of the output bar, and good agreement between the two curves was observed (e.g. Fig. 8). For the following results true-stress and strain (calculated assuming conservation of volume) are reported.

The results from compression experiments are shown in Fig. 9. These experiments show a marked increase of yield and flow stress and *apparent* elastic modulus with strain rate. Failure in both quasi-static and high-rate experiments was catastrophic; the specimen started breaking at the outer diameter due to a combination of shear, tensile and compression stresses, resulting in ultimate disintegration of the specimens. The strain to failure was higher in the high-rate experiments (55%) than in the quasi-static experiments (45%), see Fig. 10. No failure was achieved at medium rates of strain due to limitations of the loading system used.

For tensile experiments, the specimens were carefully aligned with the load axis in order to reduce bending effects; however, these are nearly impossible to completely eliminate, as reported in Ref. [7], and a comparably large scatter in failure strength measured is inevitable for all rates of loading. Analogical to the compression experiments a validity check was performed for the high-rate

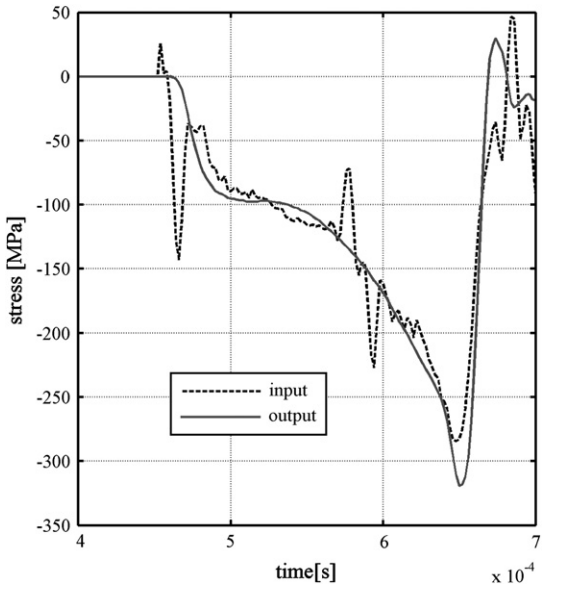

Fig. 8. Stress at ends of input and output bar as function of time for a compression specimen (example of specimen HR-C-03, 4400 s^{-1}).

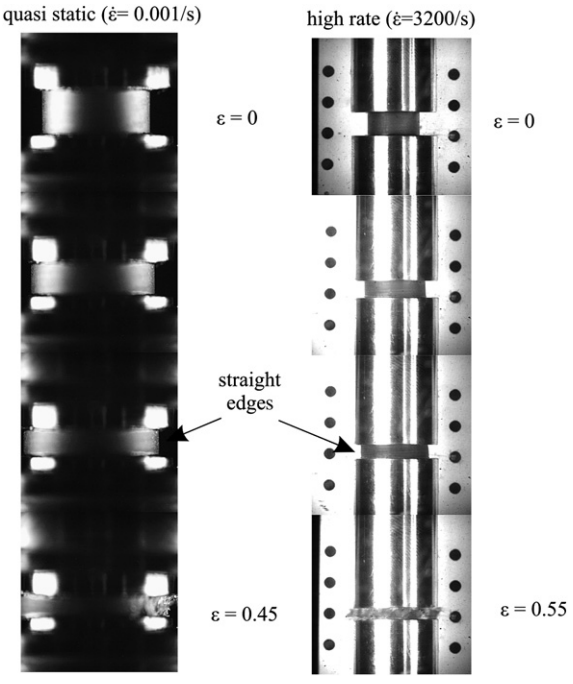

Fig. 10. Sequence of photographs of compressive experiments at quasi-static and high strain rates.

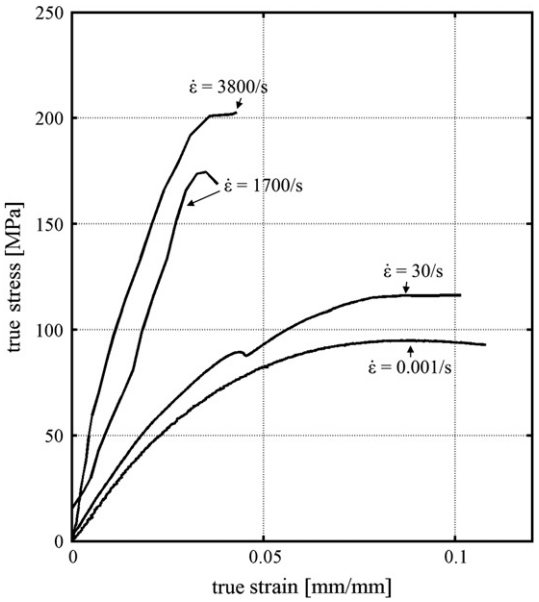

Fig. 11. Representative stress–strain curves at four selected strain rates in tension.

tension. This included a check for constancy of strain rate using a high speed camera and a check for constant strain using the speckle analysis. As a further guideline for specimen design, a stress state sufficiently close to stress equilibrium generally requires that the loading pulse travels at least three times back and forth through the specimen [8]. For the herein adopted short gauge section, this takes around 17 μs, and the time for failure of all specimens exceeded this value.

The results show a significant increase in failure strength and apparent elastic modulus with increasing strain rate, while the strain to failure decreases (Fig. 11). The fracture plane was nearly perpendicular to the loading axes in all cases. Fracture occurred in the middle of the gauge section at quasi-static and medium rates of loading (Fig. 12). During the high-rate tests, fracture could occur at one, two or more places simultaneously.

It has been argued that this could be used as an indicator for stress equilibrium [8]; however, it only proves that the maximum stress was reached at a discrete number of points along the gauge section. It seems to be more likely that this phenomenon is an inevitable result of stress wave reflections and other irregularities (such as small imperfections in specimen dimensions) that prevent perfect stress equilibrium.

The experiments were parameterised in terms of the yield stress, derived from true-stress nominal-strain curves using Considère's construction; the results are shown as a function of log strain rate in Fig. 13.

The effect of hydrostatic stresses on the material response is considerable, with the compressive yield strength being approximately 50% higher than the tensile. For modelling purposes, an apparent modulus (secant modulus to 1% strain) was also derived, and this is shown in Fig. 15. Both modulus and yield strength show a nonlinear dependency on log strain rate, with a sharp increase in gradient at a strain rate of approximately 900 s^{-1} for compression and tension alike. Results from studies performed on other polymers indicate that this increase is due to the beta relaxation process in the polymer [17,32]. The authors are aware that it is generally accepted not to be possible to derive a high strain rate modulus from standard Hopkinson bar experiments. However, the apparent modulus reported here is a pragmatic value required for modelling.

2.4. Results in 3-point bending

Fig. 14 shows typical force displacement curves for 3-point bend tests, while Table 1 summarises the results obtained. The quasi-static tests show a pronounced nonlinear behaviour; all beams failed on the tensile side of the beam, and the results confirm the high scatter for tensile strength in unidirectional tests. Although the beams were carefully machined, the ultimate deflection at failure varied considerably. For the quasi-static experiments, photography and speckle correlation were used to find the displacement field on the surface of the rod, and thus the compressive and tensile strains in the rod could be calculated. The maximum tensile strain achieved on the underside of the rod in the quasi-static experiments was 8%, compared to the 10% reached in unidirectional tensile tests.

The high speed experiments generally showed a slightly increased stiffness of the beam, as expected from the strain rate sensitivity of the beam material. The ultimate deflection was

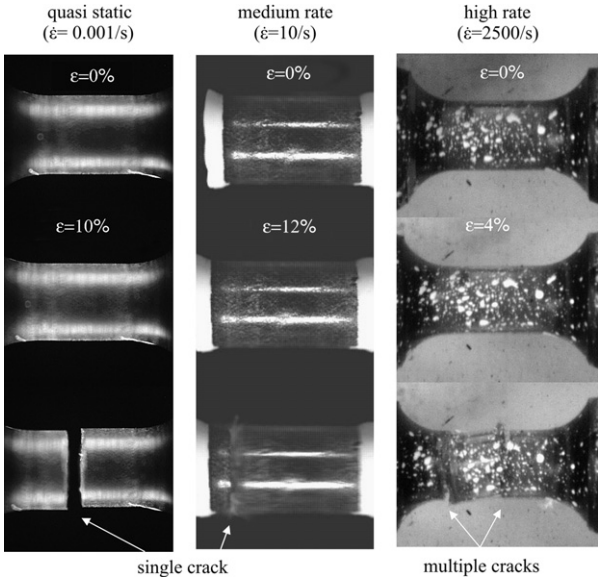

Fig. 12. Example frames showing fracture behaviour for tensile specimens at three different strain rates.

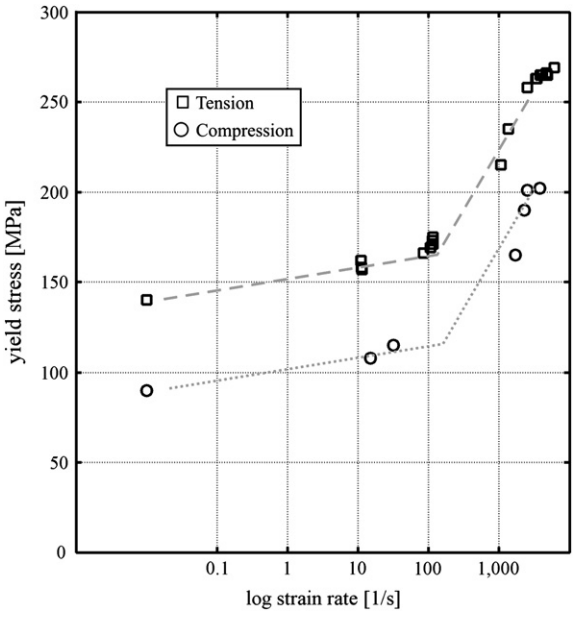

Fig. 13. Strain rate dependency of yield stress (Considère's construction).

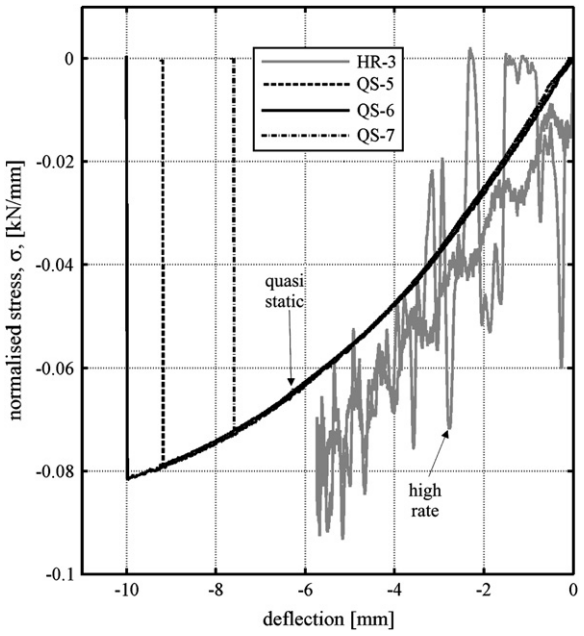

Fig. 14. Results of the quasi-static and dynamic 3-point bending tests on RTM-6. The nominal stress, σ, is calculated by dividing the force by the beam width.

considerably lower than in the quasi-static experiments. This trend is consistent with the findings from the uniaxial tensile characterisation.

3. Constitutive model

The Goldberg model is extensively described in Refs. [19–21]. It assumes that the total strain (ε^{T}) in the deformed polymer consist of an elastic (ε^{E}) and an inelastic (ε^{I}) parts:

$$\varepsilon_{ij}^{\mathrm{T}} = \varepsilon_{ij}^{\mathrm{E}} + \varepsilon_{ij}^{\mathrm{I}}. \tag{2}$$

Using the elastic strain tensor and the isotropic compliance matrix $C(E,\nu)$, the stress tensor and its deviatoric component S_{ij} can be calculated. Written in incremental notation to highlight the components that evolve with the strain/time-increment, the inelastic strain rate-tensor is

$$\dot{\varepsilon}_{ij_{(t)}}^{\mathrm{I}} = 2D_0 \exp\left[-\frac{1}{2}\left(\frac{Z_{(t)}}{\sigma_{e(t)}}\right)^{2n}\right]\left(\frac{S_{ij(t)}}{2\sqrt{J_{2(t)}}} + \alpha_{(t)}\delta_{ij}\right). \tag{3}$$

Table 1
Summary of experimental results for 3-point bending tests

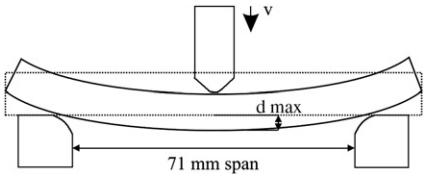

Specimen	σ_{max} [kN/mm]	d_{max}[mm]	Speed [m/s]
HR-01	–	5.70	8.0
HR-02	–	5.80	9.5
HR-03	–	5.80	5 (intact)
HR-04	–	5.60	7.0
QS-05	0.082	10.00	3.4E−06
QS-06	0.079	9.24	3.4E−06
QS-07	0.072	7.70	3.4E−06

In Eq. (6) D_0 is a material constant representing the maximum inelastic strain rate, and the constant n controls the rate dependency of the material. $J_{2(t)}$ is the absolute value of the second invariant of the deviatoric stress tensor, δ_{ij} is the Kronecker-symbol, and $\sigma_{e(t)}$ is the effective stress

$$\sigma_{e(t)} = \sqrt{3J_{2(t)}} + \sqrt{3}\alpha_{(t)}\alpha_{kk(t)} \quad \text{with} \quad \sigma_{kk(t)} = 3\sigma_{h(t)} \tag{4}$$

while $\sigma_{h(t)}$ is the hydrostatic stress. $Z_{(t)}$ is a state variable representing the resistance to molecular flow, and α is a state variable controlling the effect of hydrostatic stresses. Their evolution-equations are

$$\dot{Z}_{(t)} = q\left(Z_1 - Z_{(t)}\right)\dot{e}_{e(t)}^{\mathrm{I}}$$

$$\dot{\alpha}_{(t)} = q\left(\alpha_1 - \alpha_{(t)}\right)\dot{e}_{e(t)}^{\mathrm{I}}. \tag{5}$$

Integrating these equations leads to

$$Z_{(t)} = Z_1 - (Z_1 - Z_0)\cdot\exp\left(-q\cdot\dot{e}_{e(t)}^{\mathrm{I}}\right)$$

$$\alpha_{(t)} = \alpha_1 - (\alpha_1 - \alpha_0)\cdot\exp\left(-q\cdot\dot{e}_{e(t)}^{\mathrm{I}}\right) \tag{6}$$

with the indices 0 and 1 marking the initial and maximum values of the state variables Z and α, and q being a material constant representing the "hardening" of the material. Finally, the effective deviatoric inelastic strain rate is defined as follows:

$$\dot{e}_{e(t)}^{\mathrm{I}} = \sqrt{\frac{2}{3}\dot{e}_{ij(t)}^{\mathrm{I}}\dot{e}_{ij(t)}^{\mathrm{I}}}$$

$$\dot{e}_{ij(t)}^{\mathrm{I}} = \dot{\varepsilon}_{ij(t)}^{\mathrm{I}} - \dot{\varepsilon}_{m(t)}^{\mathrm{I}}\delta_{ij}$$

$$\dot{\varepsilon}_{m(t)}^{\mathrm{I}} = \left(\dot{\varepsilon}_{11(t)}^{\mathrm{I}} + \dot{\varepsilon}_{22(t)}^{\mathrm{I}} + \dot{\varepsilon}_{33(t)}^{\mathrm{I}}\right)/3. \tag{7}$$

The material constants that need to be determined are D_0, n, q, Z_0, Z_1, α_0 and α_1. The procedure used to define the material constants D_0, n, q, Z_0, Z_1 in this study follows the original approach [33], which uses a number of uniaxial tensile or compression tests at different strain rates to curve fit the constants. Since experimental data for shear were not available, α_0 and α_1 were obtained iteratively by comparing compressive and tensile data at the same strain rate.

3.1. Incorporation of rate dependent modulus and rate dependent failure criterion

In the original Goldberg Model, the elastic modulus is strain rate-independent. However, the purely elastic part of a polymer's mechanical response occupies only a very small region of strain, and experimental stress–strain curves show nonlinear stress–strain behaviour almost from the start of the loading. Experimental data from the literature and the experiments on RTM-6 resin within this project have shown, that this "apparent" elastic modulus (secant modulus) of glassy polymers is in fact highly strain rate dependent. This phenomenon is assumed to be of significant importance for strain rate dependent virtual testing of 3D weavings. Therefore, a simple formula to account for this strain rate dependency, as suggested in Ref. [34], has been introduced. Firstly, a linear dependence of elastic modulus $E_{lin(t)}$ on log strain rate was introduced:

$$E_{lin(t)} = E_0\left(1 + C_1 \ln\frac{\dot{\varepsilon}_{(t)}}{\dot{\varepsilon}_0}\right). \tag{8}$$

The subscript 0 denotes the initial values of the strain rate and modulus, and C_1 is scaling material constant. This modulus only feeds back into the compliance matrix. The effective strain rate is given by

$$\dot{\varepsilon}_{(t)} = \sqrt{\frac{2}{3}\left[(\dot{\varepsilon}_{11}-\dot{\varepsilon}_m)^2+(\dot{\varepsilon}_{22}-\dot{\varepsilon}_m)^2+(\dot{\varepsilon}_{33}-\dot{\varepsilon}_m)^2+2\dot{\varepsilon}_{12}^2+2\dot{\varepsilon}_{23}^2+2\dot{\varepsilon}_{13}^2\right]} \tag{9}$$

and

$$\dot{\varepsilon}_m = \frac{1}{3}(\dot{\varepsilon}_{11}+\dot{\varepsilon}_{22}+\dot{\varepsilon}_{33}). \tag{10}$$

However, the experimental results (see Fig. 13) show a marked nonlinear rate dependence of engineering properties. This needs to be taken into account by the model, and simple variation of the Weibull distribution formulation has been adopted:

$$E_{add(t)} = E_{diff}\left(1-\exp\left(C_2\left(\dot{\varepsilon}_{(t)}\right)^{C_3}\right)\right). \tag{11}$$

with both C_2 and C_3 being scaling material constants and E_{diff} representing the maximum increase of elastic modulus that can be modelled. The reason for the choice of an upper boundary for the elastic modulus is the unavailability of experimental validation data at strain rates in excess of 6000 s^{-1}. The total strain rate dependent modulus used for the modified Goldberg model is

$$E_{(t)} = E_{lin(t)} + E_{add(t)}. \tag{12}$$

The determination of the material constants C_1, C_2 and C_3 is performed using the experimentally measured apparent moduli at different strain rates (Fig. 15).

When evaluating the moduli, it is important to note that in the tensile experiments at all strain rates the specimen strain was calculated by tracking or stripes speckles applied to the specimen surface within the gauge length, using the laser extensometer for the quasi-static experiments and appropriate high speed cameras at the medium and high strain rates. On the other hand, the strain in the compressive experiments was calculated using the displacement of the anvils. This means that there was a tendency to underestimate the apparent compressive modulus, especially in the high-rate experiments where the rise time of the input and reflected pulses as well as the travel time in the specimen also play a role. Therefore, the tensile modulus must be regarded as more reliable than the compressive modulus in these data.

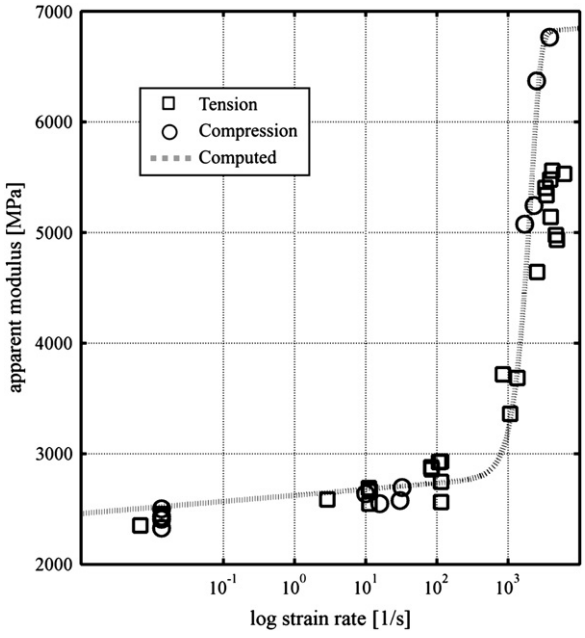

Fig. 15. Experimentally measured modulus and computed rate depended modulus incorporated into the Goldberg model.

The original Goldberg model does not include a failure criterion. In order to simulate the fundamentally different failure behaviour of RTM-6 in compression and tension, it is assumed that compression does not lead to failure, whilst the brittle response in tension is modelled. In order to differentiate between compression and tension the hydrostatic stress is used. In order to predict tensile failure, the failure criterion must be chosen taking into account the very small post-yield gradient of the stress–strain curve (close to perfect plasticity) in tensile experiments. A stress based failure criterion would lead to a very high sensitivity of the failure strain; therefore, a simple strain based formulation (maximum principal strain) for failure was chosen:

$$\varepsilon_{ets}^{T} = \sqrt{\frac{2}{3}}\cdot\sqrt{\left(\varepsilon_1^T\right)^2+\left(\varepsilon_2^T\right)^2+\left(\varepsilon_3^T\right)^2}. \tag{13}$$

The equivalent total strain ε_{ets}^{T} is, furthermore, assumed to be rate dependent, as observed in the experiments. For simplicity, the same rate dependence as observed for the modulus is used:

$$\varepsilon_{fail_{(t)}} = \varepsilon_{in} + \left(\varepsilon_{diff}\left(1-\exp\left(C_2\left(\dot{\varepsilon}_{(t)}\right)^{C_3}\right)\right)\right) \tag{14}$$

where the constants C_2 and C_3 are the same as in Eq. (11), ε_{in} is the initial failure strain, and ε_{diff} is the difference between the failure strain in quasi-static and high-rate experiments. The used material constants are shown in Table 2.

3.2. Results and model validation

The model was implemented into the FEM software LS-DYNA as a user defined material model. A comparison of the model and experimental results at different strain rates is shown in Fig. 16.

Qualitatively, the model captures the hydrostatic stress effects, the brittle response in tension, the ductile response in compression, the strain rate dependency in general and the rate dependency of the modulus and the failure strain in particular. Quantitatively, the stress–strain relationship is very well captured for quasi-static loading. At medium rates, the tensile behaviour is captured well too, while in compression, the stresses are slightly over predicted. At high rates, the model is capable of describing the compressive response reasonably well while it under predicts the tensile stresses. The tensile stress–strain

Table 2
Summary of material constants required for room temperature modelling of RTM-6 resin

Material constants for the original Goldberg model								
E_0	ν	α_0	α_1	Z_0	Z_1	n	D_0	q
2840	0.38	0.06	0.13	400	750	0.93	1×10^6	90
Material constants required for the extended model								
ε_0	E_{diff}	ε_{in}	ε_{diff}	C_1	C_2		C_3	
0.001	3500	0.1	−0.05	0.01	-1×10^{-10}		3	

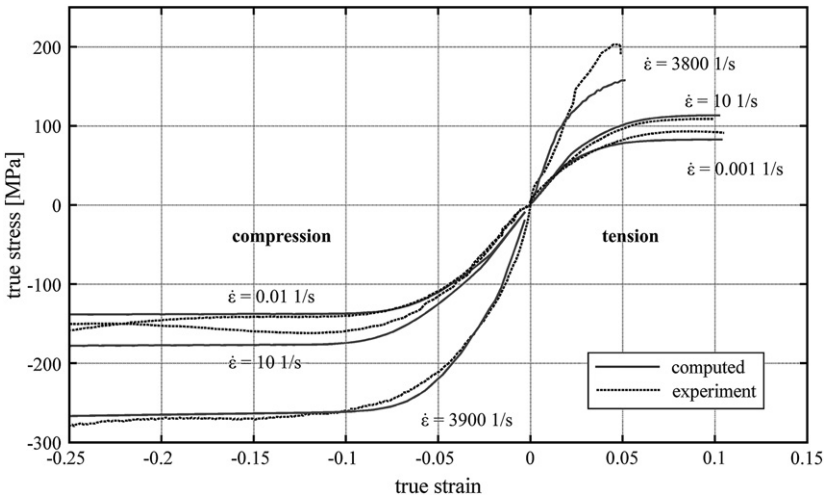

Fig. 16. Comparison of experimentally generated data against the output of the extended Goldberg model in compression and tension at different strain rates.

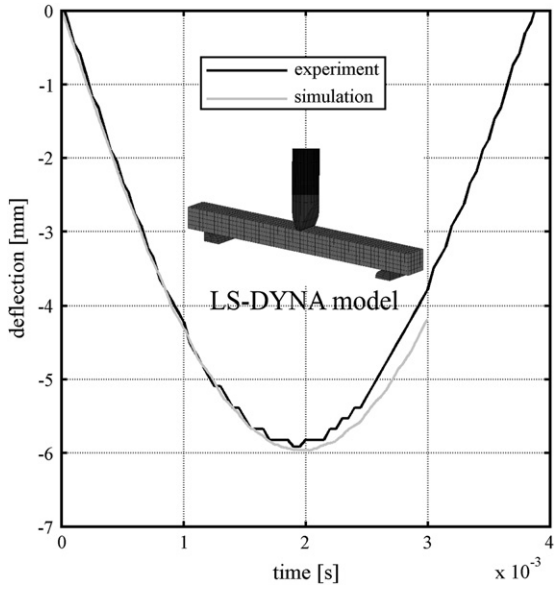

Fig. 17. Comparison of the deflections measured from high speed camera footage of a 3-point bend validation experiment against the LS-DYNA simulation (specimen HR-03, see Fig. 14).

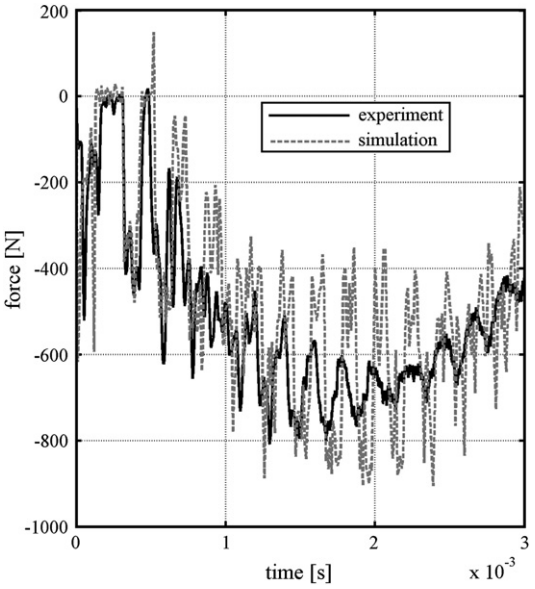

Fig. 18. Comparison of the force record from a 3-point bend validation experiment the LS-DYNA simulation (specimen HR-03, see Fig. 14).

relationship is represented very well for quasi-static and medium rates of strain, but the failure stresses at high strain rates are under-represented by roughly 20%. The experimental data suggest that in terms of the Goldberg constants the value of Z_1 should be made rate dependent for tensile behaviour, but this has not been addressed in this study.

In order to perform a large scale validation of the constitutive model, the 3-point impact bending test described in Section 2.2 was simulated. The applied boundary conditions were the initial velocity of the impactor and rigid contact between the specimen and the support (see Section 2.1). Validation consists of comparing the model output for the velocity and force at the tip of the impactor with that observed in the experiment. Figs. 17 and 18 show the results for specimen HR-03. Quantitatively the force time curve is very well captured. The displacement time curve agrees excellently with experimental results until the point of maximum deflection, subsequent differences are related to the unloading behaviour of the resin.

4. Conclusions

The results of comprehensive mechanical characterisation of the room temperature response of RTM-6 resin system at a range of strain rates have been presented. By applying a novel pulse shaping technique and improved specimen design tensile data at strain rates not yet reported in the literature were generated. Thus derived data contribute to the understanding of the observed differences between compressive and tensile behaviour at high rates of strain.

The Goldberg polymer model has been modified to comprise the observed and quantified strain rate depended stiffness. A simple fracture criterion has been added that takes the different responses in compression and tension into account. The constitutive model has been implemented into the explicit FEM software LS-DYNA, allowing for a verification of the model against experiments with complex stress states. The modified constitutive model showed an excellent agreement with the experimental data.

Acknowledgments

R. Gerlach would like to thank Rolls-Royce for funding his research, and, in particular, A. McMillan for her continued support. Furthermore, the authors kindly acknowledge funding of EPSRC and the supply of the resin RTM-6 by HEXCEL, and would like to thank S. Mortimer for his assistance, without which the project would not have been possible. Also, the support of C. P. Buckley, on different aspects of this study, has been invaluable. The Cordin 550 high speed camera used in this research was provided by the EPSRC instrument loan pool. We are particularly grateful to A. Walker for his advice and support whilst using this camera.

References

[1] Mazumdar SK. Composites manufacturing – materials, product, and process engineering. CRC Press; 2002.
[2] Staab GH. Laminar composites. Butterworth Heinemann; 1999.
[3] Peters ST. Handbook of composites. Chapman and Hall; 1998.
[4] Zhao LG, Warrior NA, Long AC. Composites Science and Technology 2006;66:36–50.
[5] Gilat A, Goldberg RK, Roberts GD. Journal of Aerospace Engineering 2007;20:75–89.
[6] Chen W, Zhou B. Mechanics of Time-Dependent Materials 1998;2:103–11.
[7] Buckley CP, Harding J, Hou JP, Ruiz C, Trojanowski A. Journal of the Mechanics and Physics of Solids 2001;49:1517–38.
[8] Chen W, Lu F, Cheng M. Polymer Testing 2002;21:113–21.
[9] Khan MZS, Simpson G, Townsend CR. Materials Letters 2002;52:173–9.
[10] Pyttel T, Weyer S. International Journal of Crashworthiness 2003;8:433–42.
[11] Duan Y, Saigal A, Greif R. Polymer Engineering and Science 2003;43:112–24.
[12] Rager A, Williams JG, Ivankovic A. International Journal of Fracture 2005;135:199–215.
[13] Wiegand J, Petrinic N. VITAL material down-selection by 3 point bending test. In: Internal-Report 228. Department of Engineering, University of Oxford; 2006.
[14] Young RJ, Lovell PA. Introduction to polymers. London: Chapmann and Hall; 1991.
[15] Ward IM, Sweeney J. An introduction to the mechanical properties of solid polymers. Wiley; 2004.
[16] Porter D. Group interaction modelling of polymer properties. New York: Marcel Dekker; 1995.
[17] Mulliken AD, Boyce MC. International Journal of Solids and Structures 2006;43:1331–56.
[18] Buckley CP, Dooling PJ, Harding J, Ruiz C. Journal of the Mechanics and Physics of Solids 2004;52:2355–77.
[19] Goldberg RK, Roberts GD, Gilat A. Composites Part B: Engineering 2003;34:151–65.
[20] Goldberg RK, Roberts GD, Gilat A. Journal of Aerospace Engineering 2005;18:18–27.
[21] Goldberg RK, Stouffer DC. Journal of Composite Materials 2002;36:773–93.
[22] Gilat A, Goldberg RK, Roberts GD. Strain rate sensitivity of epoxy resin in tensile and shear loading. NASA/TM-2005–213595; 2005.
[23] Gorham DA. Journal of Physics D – Applied Physics 1989;22:1888–93.
[24] Harding J, Welsh LM. Journal of Materials Science 1983;18:1810–26.
[25] Sjödahl M. Applied Optics 1994;33:6667–73.
[26] Sjödahl M, Benckert LR. Applied Optics 1993;32:2278–84.
[27] Hallett SR. Composites Science and Technology 2000;60:115–24.
[28] Awaji H, Sato S. Journal of Engineering Materials and Technology 1979;101:139–47.
[29] Grantham SG, Siviour CR, Proud WG, Field JE. Measurement Science and Technology 2004;15:1867–70.
[30] Frew DJ, Forrestal MJ, Chen W. Experimental Mechanics 2002;42:93–106.
[31] Parry DJ, Walker AG, Dixon PR. Measurement Science and Technology 1995;6:443–6.
[32] Siviour CR, Walley SM, Proud WG, Field JE. Polymer 2005;46:12546–55.
[33] Goldberg RK, Stouffer DC. NASA/TM-1998-206969; 1998.
[34] Zheng X. Nonlinear strain rate dependent composite model for explicit FEM analysis. Ph.D. Thesis. University of Akron; 2006.